Materialia 21 (2022) 101307

Contents lists available at ScienceDirect

Materialia

journal homepage: www.elsevier.com/locate/mtla

The preexisting edge dislocations as recombination center of point defects enhancing irradiation tolerance in CoCrCuFeNi high entropy alloy

Yu Liu[a], Rui Li[a,*], Qing Peng[b,*]

[a] School of Mechanical Engineering, University of Science and Technology Beijing, Beijing, 100083, China
[b] State Key Laboratory of Nonlinear Mechanics, Institute of Mechanics, Chinese Academy of Sciences, Beijing 100190, China

ARTICLE INFO

Keywords:
High entropy alloys
Irradiation resistance
Cascade
Dislocation
Void

ABSTRACT

Defect clusters including dislocations, grain boundaries, and precipitations can serve as sink sources for point defects during radiation damage. As a result, radiation tolerance can be tuned by engineering the defects in the structural materials, however, is a challenging topic due to the complexity. In this paper, the mechanism of interaction between the preexisting dislocation and the displacement cascade in CoCrCuFeNi high entropy alloy (HEA) is investigated using molecular dynamics simulations. The results show that the dislocation climbs, and promotes the diffusion of point defects generated by the cascade to the dislocation line. As a result, it increases the probability of defect annihilation and recombination and therefore strengthens radiation tolerance. The interaction of dislocations with void in CoCrCuFeNi and Ni shows that CoCrCuFeNi high entropy alloy has excellent resistance to irradiation hardening. Our atomic insights could be beneficial in the design of high-performance irradiation resistant high entropy alloys.

1. Introduction

Green energy is critical to the environment on earth and sustainable development of human being civilization. Nuclear energy plays an important role in all the strategies to generate clean energy [1]. With the development of a new generation of nuclear reactors, structure materials work in severe conditions, which demand higher irradiation resistance under high temperature. New structural materials need to be designed to meet the demands. HEAs are one potential candidate. HEAs, which are alloys with equal or nearly equal atomic ratios composed of five or more elements, were first proposed by Yeh et al. [2] and Cantor et al. [3] in 2004. Due to the severe lattice distortion [4,5], HEAs have excellent mechanical properties, such as high strength [6], high hardness [7] and high ductility [8]. Also for having slow diffusion effect [9–11], researchers suggested that HEAs might have excellent resistance to irradiation.

There are a few efforts in the study of radiation response of HEAs. Yang et al. [12] investigated the irradiation response of $Al_xCoCrFeNi$ (x = 0.1, 0.75, and 1.5) HEA. The results showed that $Al_{0.1}CoCrFeNi$ exhibited good phase stability under ion irradiation due to the high conformational entropy and atomic slow diffusion effect. Zhang et al. [13] found that the FCC phase remained stable in nanocrystalline CoCrCuFeNi at 3 MeV Ni ions irradiation at room temperature. Kumar et al. [14] investigated irradiation resistance of 27%Fe-28%Ni-27%Mn-18%Cr HEA under 5.8 MeV Ni ions at room temperature to 700 ˚C. The results showed that the dislocation loops at all temperatures were small and no voids appeared due to relatively sluggish solute diffusion. Tunes et al. [15] studied the irradiation resistance of FeCrMnNi HEA and austenitic stainless steel AISI-348 under 40 and 140 dpa doses Xe^+ heavy ions irradiation. The results showed that HEA maintained 80% of the solid solution phase, while irradiation-induced precipitation (RIP) was observed in austenitic stainless steel. Saikumaran et al. [16] found that CrFeMoV had better He ions irradiation resistance than P91 ferritic steel at room temperature. Recently, researchers found that the introduction of dislocations [17,18] and grain boundaries [19–21] in materials had a significant impact on the defects produced by cascading. For example, Lu et al. [22] indicated that dislocations promoted the formation of voids in NiCoCrFePd. Meanwhile, Cao et al. [23] studied the irradiation resistance of $(CoCrFeNi)_{94}Ti_2Al_4$ by 4 MeV Au ions at room temperature. The results showed that the presence of nano precipitates slowed down the growth of dislocation loops and the material hardening caused by irradiation was not obvious.

In addition to experiments, computations including molecular dynamics (MD) simulations have been widely used to study irradiation damage in alloys [24–27]. However, only some researchers studied the influence of dislocation on irradiation resistance in ternary and binary alloys. Dou et al. [28] investigated the interaction of edge dislocations with void in $Fe_{10}Ni_{20}Cr$ and $Fe_{33}Ni_{33}Cr$, and indicated that the latter ex-

* Corresponding author.
E-mail addresses: lirui@ustb.edu.cn (R. Li), pengqing@imech.ac.cn (Q. Peng).

https://doi.org/10.1016/j.mtla.2021.101307
Received 12 December 2021; Accepted 22 December 2021
Available online 26 December 2021

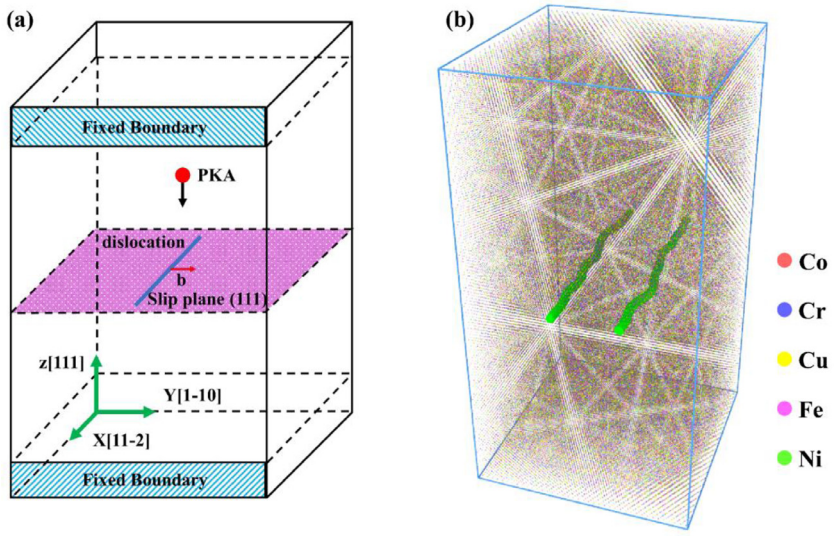

Fig. 1. Schematics of atomic models. (a) Pre-added dislocation (blue straight line) and the initial PKA position and direction. (b) CoCrCuFeNi model with random distributions, the elements are distinguished by the colors.

hibited better irradiation hardening resistance behavior due to stronger slow diffusion that would inhibit the transformation of void to stacking fault tetrahedra. Zhao et al. [29] simulated the interaction between vacancies and dislocation in pure Ni and NiFe alloys. Avalos et al. [30] investigated the change of the dipole of an edge dislocation during the cascade by molecular dynamics simulation and found that larger clusters of vacancies are produced in the presence of dislocations.

Although HEAs are proposed as novel candidates for nuclear reactor structural materials [31], the mechanism of the influence of the dislocation on irradiation resistance still lacks, therefore, in this paper, we investigate the interaction of primary knock-on atoms (PKA) with dislocations in CoCrCuFeNi HEA by molecular dynamics simulation. The approach of MD simulation is employed here because it has been proved to be suitable for displacement cascade simulations [32–34]. Our study has discovered that the pre-existing dislocations serve as defect traps absorbing irradiated defects. The model and details of molecular dynamics simulations are scrutinized in Section 2. The results and discussions are in Section 3, followed by the conclusions in Section 4.

2. Model and simulation

A 1/2<110> edge dislocation is created in the middle of the model [35], as shown in Fig. 1(a). The three directions of the Cartesian coordinate system represent the $[11\bar{2}]$, $[1\bar{1}0]$, and [111], respectively. Therefore, the Burgers vector **b** is along *y*-axis and the slip plane is perpendicular to *z*-axis. The model of CoCrCuFeNi is illustrated in Fig. 1(b), which consists of five elements of Co, Cr, Cu, Fe, and Ni with the same ratio. The model contains 186,624 atoms with dimensions of 10.4 nm × 10.2 nm × 19.7 nm along *x, y*, and *z* direction. The periodic boundary is applied along *x, y* directions [36]. Five rows of atoms at the top and bottom along z direction are fixed to avoid the movement of the model during the cascade.

Considering the size of the model, the energy of the PKA atom is chosen to be 5 keV, and the velocities are along the negative direction of *z* direction, thus the cascade interacts with a larger range of pre-added dislocation [37]. The whole simulation is performed at a temperature 300 K. The PKA locates at a distance of −1 to 5 nm from the initial dislocation at 1 nm intervals, respectively. We carry out 5 simulation cases for each PKA location, and also carry out 10 cascades for the pristine material without initial dislocation. The whole process is conducted using LAMMPS molecular dynamics software [38]. The interaction among atoms is described by EAM potential proposed by Deluigi et al. [39], which has been shown to study the cascade collision process of CoCrCuFeNi HEA successfully.

The simulation is performed as follows: First, a lattice parameter of 0.3552 nm [40] for CoCrCuFeNi is chosen, which is close to the experimental value of 0.3579 nm [41]. Then the system is relaxed at 300 K for 60 ps using NVT ensemble to make the system reach equilibrium. As shown in Fig. 1(b), due to the high energy of the initially added full dislocation, the dislocation spontaneously turns into two Shockley dislocations during relaxation: $\frac{1}{2}[0\bar{1}\bar{1}] \rightarrow \frac{1}{6}[\bar{1}\bar{1}2] + \frac{1}{6}[1\bar{2}\bar{1}]$. When the cascade collision starts, the NVE ensemble is applied. Meanwhile, the atoms in the outermost 0.5 nm thick layer of the model are selected to keep the temperature at 300 K using the Berendsen method. The other atoms are thermodynamic. An adaptive variable step is applied to ensure that the atoms do not move more than 0.002 nm within a step. The entire process lasts 100 ps, which is long enough for the model to reach equilibrium. The analysis of the simulation results is all performed using OVITO visualization software [42].

Wigner-Seitz defect analysis is applied to identify point defects generated by the cascade. The point defects consist of two parts, as shown as Fig. 2. One part is the initially added dislocations and new dislocations linked to the initial dislocations, marked with black circles in Fig. 2. Ab-SIAs and ab-Vacs denote interstitials and vacancies in this part, respectively. The other part is the rest of defects in the matrix. *Re*-SIAs and re-Vacs denote interstitials and vacancies in the matrix, respectively.

3. Results and discussions

3.1. Defects creation in cascade

With displacement cascade, PKA in CoCrCuFeNi creates plenty of Frenkel pair (FP) point defects. Defects caused by PKA will interact with the dislocation. The interaction depends on the separation between PKA and dislocation. As shown in Fig. 3(a), the interstitials (re-SIAs) and vacancies (re-Vacs) resided in the matrix are almost the same as in the ideal bulk material when the PKA occurs at −1 nm to the dislocation, which indicates that the cascade does not interact with the dislocations. However, when the distance between PKA and the initial dislocation increases is at 0–3 nm, the number of re-SIAs and re-Vacs in the matrix is less than that in the ideal material, which indicates that the dislocations act as defect traps to capture point defects. The total number of re-SIAs and re-Vacs increases gradually to that of ideal bulk material when the distance is larger than 3 nm, suggesting that the interaction between PKA and dislocation decreases.

We have examined the number of interstitials (ab-SIAs) and vacancies (ab-Vacs) that interact with dislocation, as shown in Fig. 3(b). The trend of the absorbed defects as a function of the distance is opposite to

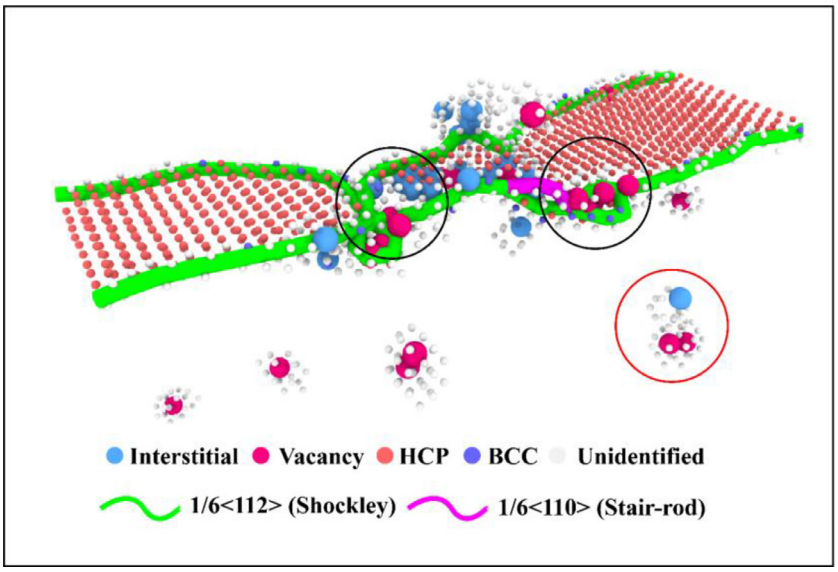

Fig. 2. Changes in atomic and dislocation structures at the end of the cascade. Interstitials and vacancies are identified using Wigner-Seitz. HCP, BCC and Unidentified are atomic structures. FCC structures have been removed.

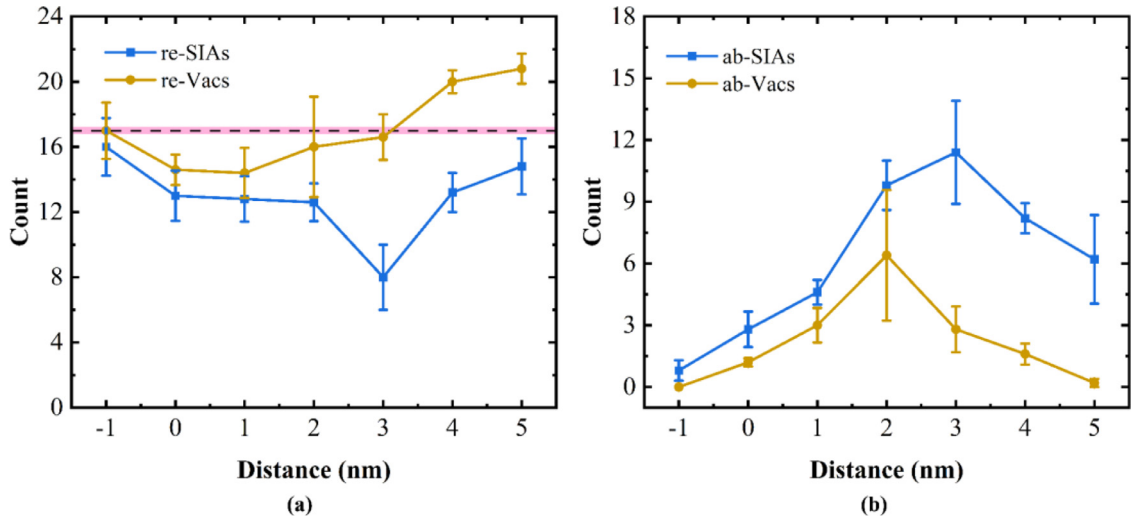

Fig. 3. The number of point defects produced by PKA with preexisting dislocation at different distances. (a) The number of point defects resided in the matrix. The black dashed line filled with light purple represents the number of defects produced by PKA in ideal bulk material. *Re*-SIAs and re-Vacs are the interstitials and vacancies resided in the matrix. (b) The number of point defects absorbed by dislocations. ab-SIAs and ab-Vacs are the interstitials and vacancies interacted with the dislocations.

that of residues in the matrix shown in Fig. 3(a). The peaks of ab-SIAs and ab-Vacs are at 3 nm and 2 nm, respectively. The total number of absorbed interstitials and vacancies (ab-SIAs + ab-Vacs) is the biggest at 2 nm, which indicates that the dislocation absorbs the most point defects at this distance.

The number of vacancies resided in the matrix is larger than the number of interstitials (Fig. 3(a)), which implies that the dislocations tend to capture more interstitials. A large number of vacancies might gather to form void and thus lead to swelling. To check this hypothesis, the distribution of residual defect clusters in the matrix is analyzed when the distance between PKA and dislocation is at −1 nm, 2 nm and 3 nm. The cascade does not interact with dislocation at −1 nm, while the interaction between PKA and dislocation is the strongest at 2 nm and 3 nm. As shown in Fig. 4(a), the residual interstitial clusters in the matrix are mainly dominated by sizes 1 and 2 at 2 nm and 3 nm. There are much more interstitial clusters of sizes 3–5+ in the bulk, and when the seperation of PKA and dislocation is −1 nm. More importantly, there is no cluster of size of 5+ when the distance is 3 nm. The vacancy clusters in Fig. 4(b) also show that the vacancy cluster size 1 dominates at distance 3 nm, and there is no big cluster whose size is larger than 5. The results imply that the absorption of point defects by dislocations in CoCrCuFeNi can reduce the formation of large defect clusters in the matrix.

3.2. The dislocation during pka process

At the end of the cascade process, the point defects aggregate to form various defect clusters including dislocations. The dislocation number density and dislocation density are analyzed as shown as Fig. 5(a)-(b). Both dislocation number density and dislocation density at distance 2 nm and 3 nm increase gradually, and then fluctuate within a certain range. The number density and dislocation density at distance −1 nm is obviously less than the cases in which PKA interacts with dislocation. Besides, the dislocation density fluctuates to a less extent than the dislocation number density in three cases, consistent with the results of Peng et al. for the Fe simulation cascade [32]. The average dislocation length is shown in Fig. 5(c). The −1 nm, 2 nm and 3 nm cases have an average dislocation length of 10.6 nm in the beginning because of the

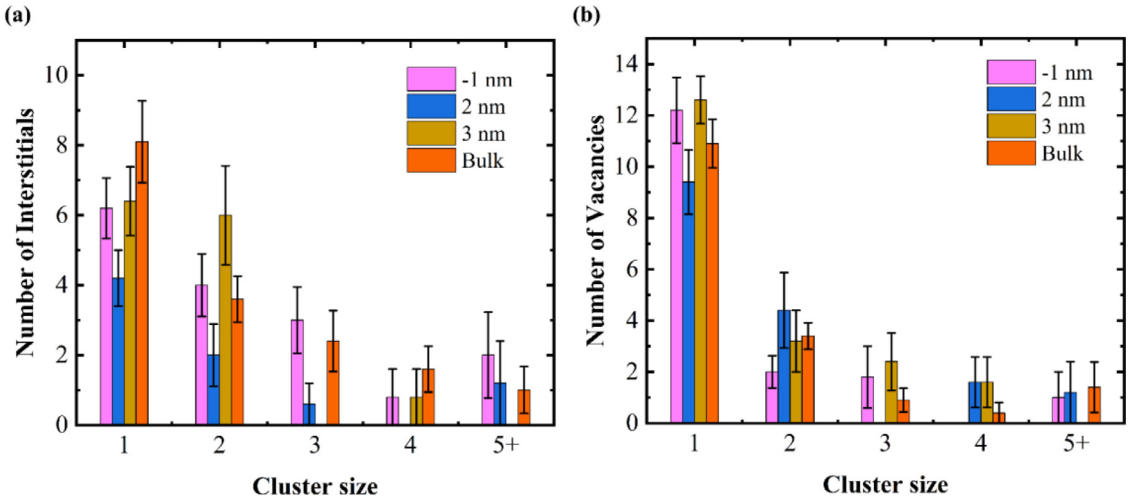

Fig. 4. The size distribution of the defect clusters during displacement cascade. −1, 2, 3 nm represents the distance between PKA and dislocation. Bulk denotes the ideal material without dislocation. (a) The number of interstitials in clusters of different sizes. (b) The number of vacancies in clusters of different sizes.

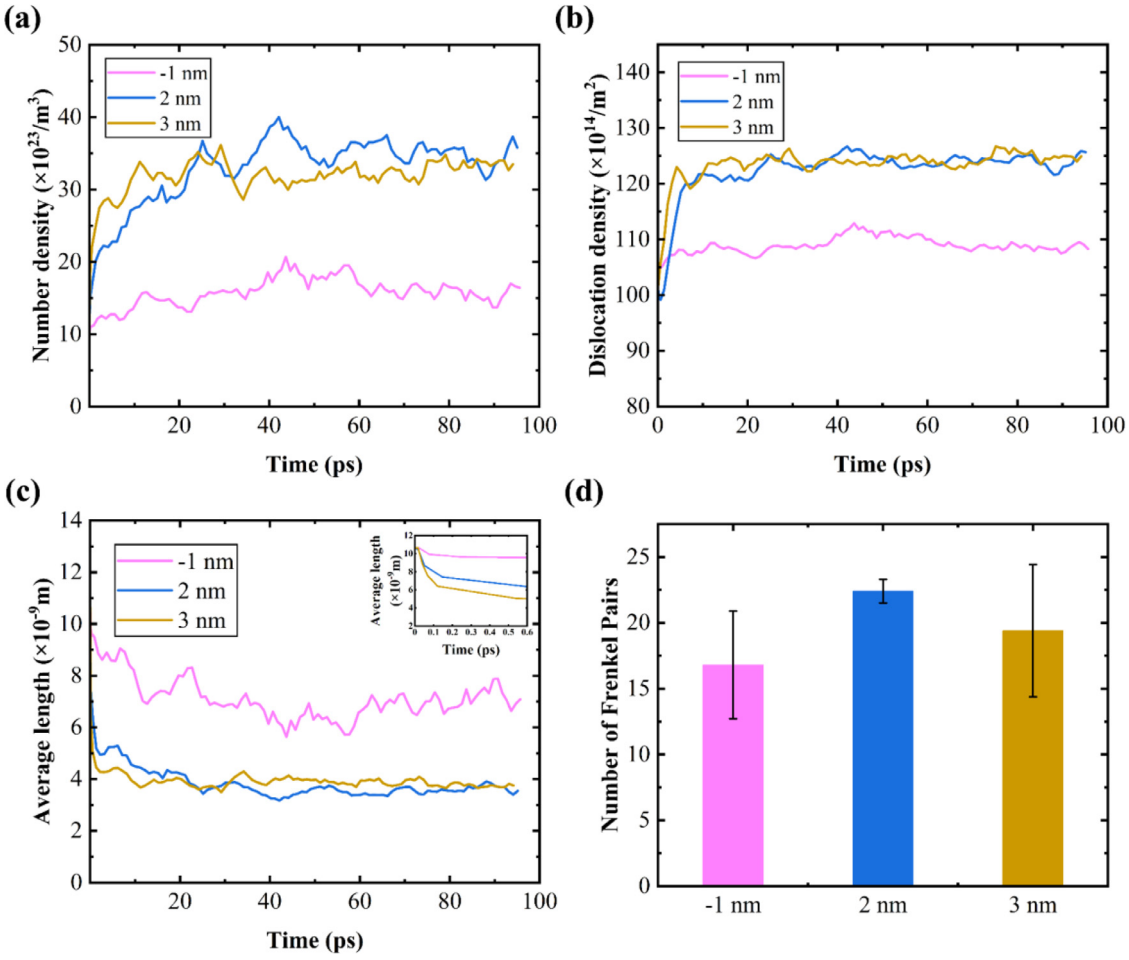

Fig. 5. Dislocations. (a) Dislocation number density. (b) Dislocation density. (c) Average length of dislocation, the inset shows the zoo-in view for better comparison. (d) Total number of point defects produced in PKA with distance −1, 2, and 3 nm.

initial addition of edge dislocations. When the cascade begins, the average dislocation length decreases rapidly in cases with distance 2 and 3 nm. The dislocation length is largest in the case with distance −1 nm. The results imply that the interaction between cascade and dislocation increases the dislocation density in the material, but decrease the average dislocation length. The total number of defects (re-SIAs + ab-SIAs) in these three cases is shown in Fig. 5(d). Fewer point defects are produced in the case with distance −1 nm than that in 2 and 3 nm, which is consistent with the conclusion.

The discussion above compares the variation in point defects and dislocations. Now we focus on how the pre-added dislocations absorb the point defects. As shown in Fig. 6(a), the number of defects reaches the

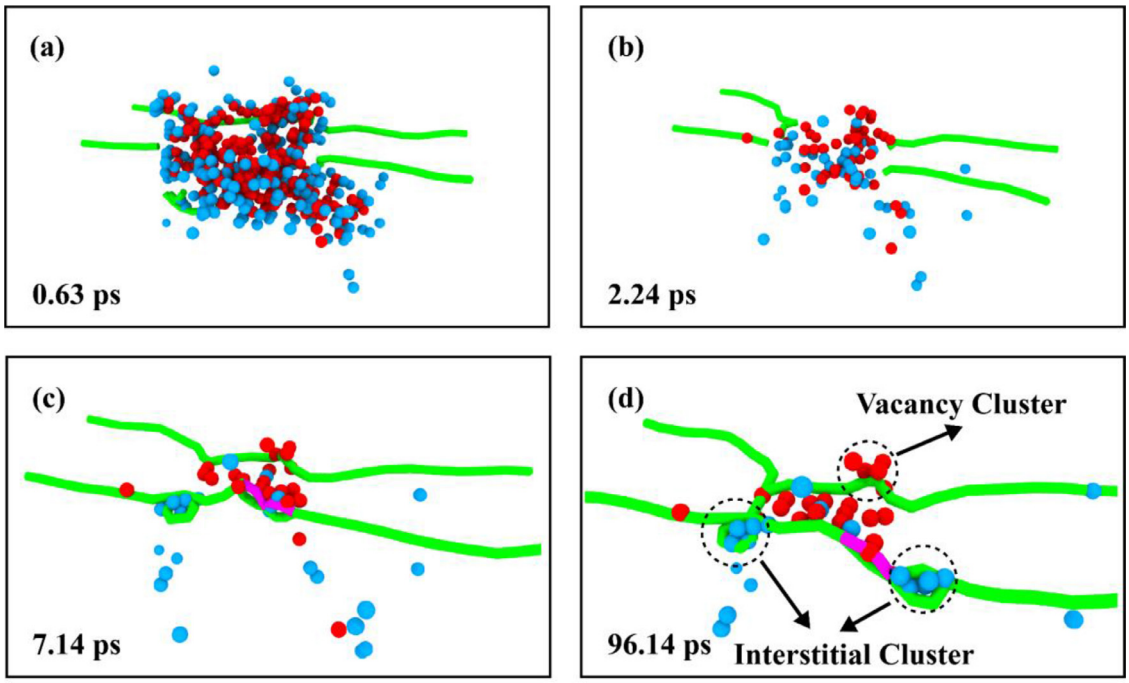

Fig. 6. Evolution of dislocations and point defects during cascade in CoCrCuFeNi. Different color lines denote different dislocations, Green, purple are 1/6<112> Shockley dislocation, 1/6<110> Stair-rod dislocation, respectively, Red and blue spheres are vacancies and interstitials, respectively.

maximum value at 0.63 ps. When the displacement cascade proceeds to 2.24 ps, the number of defects reduces obviously due to annihilation. Shockley dislocation can only slip but not climb. When the leading dislocation of these two dislocations encounters an obstacle and stops slipping, while the tracking dislocation continues slipping until the two dislocations overlap and form a full dislocation, and then it can climb. As shown in Fig. 6(c), The cascade interacts with the leading dislocation to form an L-C dislocation: $\frac{1}{6}[\bar{2}\bar{1}\bar{1}] + \frac{1}{6}[121] \rightarrow \frac{1}{6}[\bar{1}10]$, also known as Stair-rod dislocation, which is a fixed dislocation that cannot slip. It therefore hinders the slippage of the leading dislocation in the Shockley dislocations.

Fig. 6(d) shows the tracking dislocation catches up with the leading dislocation and overlaps each other, so that the two Shockley dislocations achieve climbing. When the vacancy and interstitial spread from elsewhere to the dislocation line, they are called positive and negative climbing. Dislocations absorb vacancies by positive climbing and interstitials by negative climbing, thus reduce the number of point defects in the matrix. At the same time, the interstitials and vacancies captured by dislocations have the opportunity to undergo annihilation.

3.3. Interaction of dislocation and void

when the cascade generates a large number of vacancies aggregation, void forms, which can cause serious damage to the material. Therefore, it is necessary to study the interaction of dislocation with void driven by external loads such as shear strain. Meanwhile, the study shows that HEAs may have better resistance to irradiation than simple alloys [14,15,27]. Here we compare the interaction of dislocations with void in CoCrCuFeNi HEA and Ni to investigate irradiation hardening resistance of HEAs.

First, a 0.8 nm diameter void is set in the middle of the model. The upper and lower 0.6 nm thick atomic layers are set as rigid. The 0.7 nm thick atomic layers adjacent to the rigid bodies are set as thermostatic layers. The void is far enough from the initial dislocations so that the dislocations do not interact with it during relaxation. The temperature is 500 K. Besides, to allow a large enough shear speed for the dislocations, a shear strain rate of $6 * 10^7\ s^{-1}$ is applied to the upper rigid body. The results show that the width of the stacking fault in CoCrCuFeNi HEA is larger than in Ni, which means $L_1 < L_2$, as shown as Fig. 7(a) and (e). The width of stacking fault is related to the stacking fault energy

$$L_0 = \frac{Ga^2}{24\pi\gamma_1} \tag{1}$$

where G is shear modulus, a is the lattice constant, γ_1 is the stacking fault energy. The stacking fault energies in two cases are calculated. The HEAs have random distribution of atoms in the stacking fault region due to the complexity of their composition. We create a model of 100 CoCrCuFeNi HEA to calculate the distribution of the stacking fault energies. The results are shown in Fig. 8(a). The mean value μ obtained by Gaussian fitting is 67.15 mJ/m^2, while the stacking fault energy of Ni is a definite value of 124.55 mJ/m^2, which explains the larger width of the stacking fault region in CoCrCuFeNi HEA than that in Ni according to Eq. 1.

When the shear is applied, the dislocations move towards the direction of the void, as shown in Fig. 7(b)-(d) and (f)-(h) for the interaction of dislocations and void during the whole process. It is noteworthy that the void in Ni has been partially transformed into stacking fault tetrahedra in the region, while the void in the HEA remains stable. Fig. 7(d) and (h) also show that part of the void in Ni has formed stacking fault tetrahedra after interacting with dislocations, while the voids in the CoCrCuFeNi HEA remain the same. The shear stress τ_{zx} during the whole process are shown in Fig. 8(b). Since the void is hard to move, the movement of the dislocation is hindered by the void and therefore the value of the shear stress reaches its minimum in the Ni and HEA, as shown in C_1 and N_1 in Fig. 8(b) corresponding to Fig. 7(b) and (f). The stress peaks occur at N_2 and C_2 when the dislocation totally go through the void, as shown as Fig. 7(c) and (g). The shear stress is 331.5 MPa and 195.1 MPa in Ni and CoCrCuFeNi, respectively, indicating the stacking fault tetrahedra have a stronger hindering effect on the dislocations in Ni. The results imply that CoCrCuFeNi HEAs have excellent resistance to irradiation hardening.

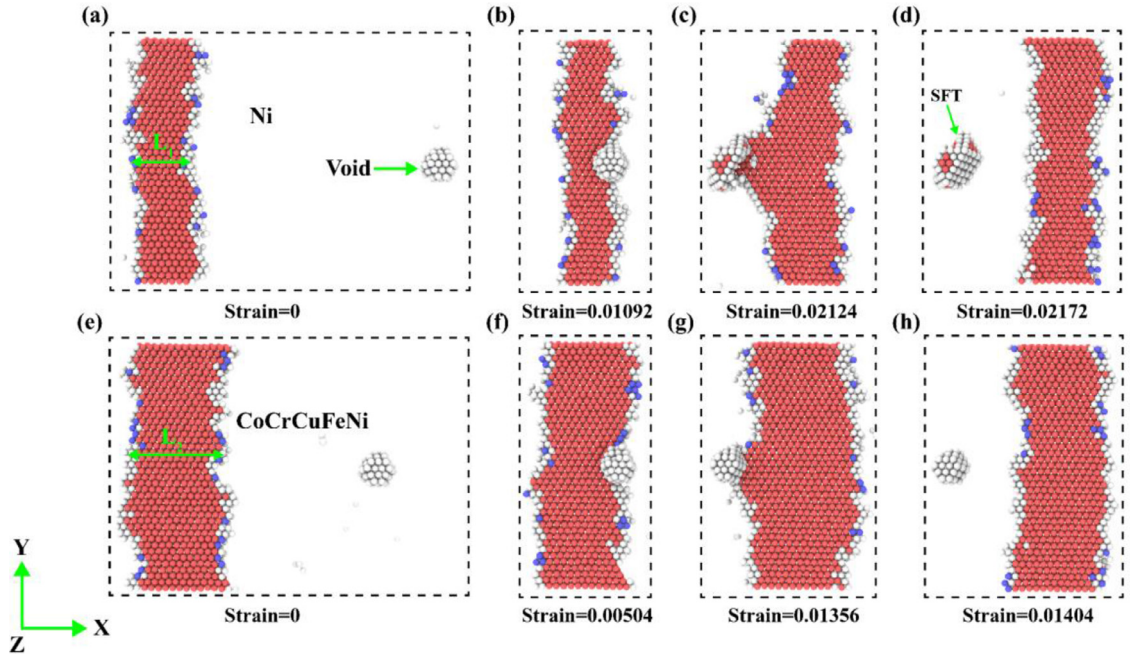

Fig. 7. Interaction of the pre-added dislocations with the void. (a)-(d) Snapshot of the interaction of dislocations and voids in Ni under an applied shear strain in the x-direction. (e)-(f) Snapshot of the interaction of dislocations and voids in CoCrCuFeNi under applied shear strain in the x-direction, the types of atoms of different colors are consistent with Fig. 2, here the hollow spheres made up of white atoms represent voids.

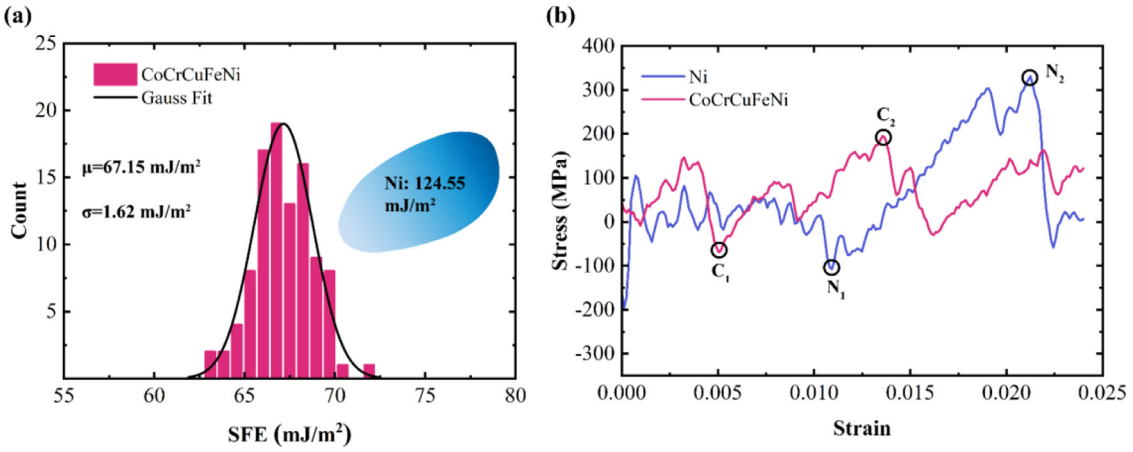

Fig. 8. (a) Statistic distribution of stacking fault energy in CoCrCuFeNi with mean μ and standard deviation σ obtained from Gauss fit. (b) Stress-strain curves during the interaction of dislocations and void in CoCrCuFeNi HEA compared to that in Ni.

4. Conclusions

We have investigated the effect of preexisting dislocations on the radiation resistance in CoCrCuFeNi HEA employing molecular dynamics simulations. The interaction of pre-existing dislocations with the displacement cascades depends on the seperation between the PKA and dislocations. Fewer defects remain in the matrix when the cascade generated by PKA interacts with the pre-existing dislocations. Atomic structure analysis shows that some point defects are absorbed by the dislocations. The preexisting dislocations serve as sinks for the point defects, both interstitials and vacancies.

The dislocation evolution indicates that the absorption of the point defects generated by the cascade is mainly caused by the climbing of dislocations. Preexisting dislocation can be a defect trap and the center for the recombination of point defects. The comparative study of the Ni and CoCrCuFeNi HEA systems for the interaction between dislocations and void manifests that HEAs have excellent resistance to irradiation hardening. Our atomic insights might be helpful in material design of next generation of nuclear materials with high radiation tolerance.

Declaration of competing interest

The authors declare that they have no known competing financial interests or personal relationships that could have appeared to influence the work reported in this paper.

Acknowledgments

The work is supported by Fundamental Research funds for the Central Universities (FRF-IDRY-20–008 and FRF-AT-20–09). Q. P. would like to acknowledge the support provided by LiYing Program of the Institute of Mechanics, Chinese Academy of Sciences (E1Z1011001).

References

[1] R.B. Duffey, Sustainable futures using nuclear energy, Progress in Nuclear Energy 47 (2005) 535–543.
[2] J. Yeh, S. Chen, S. Lin, J. Gan, T. Chin, T. Shun, C. Tsau, S. Chang, Nanostructured high-entropy alloys with multiple principal elements: novel alloy design concepts and outcomes, Adv Eng Mater 6 (2004) 299–303.
[3] B. Cantor, I.T.H. Chang, P. Knight, A.J.B. Vincent, Microstructural development in equiatomic multicomponent alloys, Materials Science and Engineering: A 375 (2004) 213–218.
[4] D.B. Miracle, O.N. Senkov, A critical review of high entropy alloys and related concepts, Acta Mater 122 (2017) 448–511.
[5] Z. Wang, Q. Fang, J. Li, B. Liu, Y. Liu, Effect of lattice distortion on solid solution strengthening of BCC high-entropy alloys, Journal of Materials Science & Technology 34 (2018) 349–354.
[6] D.G. Shaysultanov, G.A. Salishchev, Y. v Ivanisenko, S. v Zherebtsov, M.A. Tikhonovsky, N.D. Stepanov, Novel Fe36Mn21Cr18Ni15Al10 high entropy alloy with bcc/B2 dual-phase structure, J Alloys Compd 705 (2017) 756–763.
[7] T.-.T. Shun, C.-.H. Hung, C.-.F. Lee, The effects of secondary elemental Mo or Ti addition in Al0. 3CoCrFeNi high-entropy alloy on age hardening at 700 C, J Alloys Compd 495 (2010) 55–58.
[8] S.-.H. Joo, H. Kato, M.J. Jang, J. Moon, C.W. Tsai, J.W. Yeh, H.S. Kim, Tensile deformation behavior and deformation twinning of an equimolar CoCrFeMnNi high--entropy alloy, Materials Science and Engineering: A 689 (2017) 122–133.
[9] K.-.Y. Tsai, M.-.H. Tsai, J.-.W. Yeh, Sluggish diffusion in Co–Cr–Fe–Mn–Ni high-entropy alloys, Acta Mater 61 (2013) 4887–4897.
[10] M. Vaidya, S. Trubel, B.S. Murty, G. Wilde, S. v Divinski, Ni tracer diffusion in CoCrFeNi and CoCrFeMnNi high entropy alloys, J Alloys Compd 688 (2016) 994–1001.
[11] J.-.W. Yeh, Physical metallurgy of high-entropy alloys, Jom 67 (2015) 2254–2261.
[12] T. Yang, S. Xia, S. Liu, C. Wang, S. Liu, Y. Fang, Y. Zhang, J. Xue, S. Yan, Y. Wang, Precipitation behavior of Al x CoCrFeNi high entropy alloys under ion irradiation, Sci Rep 6 (2016) 1–8.
[13] Y. Zhang, M.A. Tunes, M.L. Crespillo, F. Zhang, W.L. Boldman, P.D. Rack, L. Jiang, C. Xu, G. Greaves, S.E. Donnelly, Thermal stability and irradiation response of nanocrystalline CoCrCuFeNi high-entropy alloy, Nanotechnology 30 (2019) 294004.
[14] N.A.P.K. Kumar, C. Li, K.J. Leonard, H. Bei, S.J. Zinkle, Microstructural stability and mechanical behavior of FeNiMnCr high entropy alloy under ion irradiation, Acta Mater 113 (2016) 230–244.
[15] M.A. Tunes, G. Greaves, H. Bei, P.D. Edmondson, Y. Zhang, S.E. Donnelly, C.G. Schön, Comparative irradiation response of an austenitic stainless steel with its high-entropy alloy counterpart, Intermetallics 132 (2021) 107130.
[16] A. Saikumaran, R. Mythili, P. Magudapathy, C. David, Comparison of Irradiation-Induced Hardening Behavior of P91 Ferritic Martensitic Steel and CrFeMoV High-Entropy Alloy, J Mater Eng Perform 30 (2021) 3547–3555.
[17] C. Lu, T.-.N. Yang, K. Jin, G. Velisa, P. Xiu, Q. Peng, F. Gao, Y. Zhang, H. Bei, W.J. Weber, Irradiation effects of medium-entropy alloy NiCoCr with and without pre-indentation, Journal of Nuclear Materials 524 (2019) 60–66.
[18] R.E. Voskoboinikov, MD simulations of collision cascades in the vicinity of a screw dislocation in aluminium, Nuclear Instruments and Methods in Physics Research Section B: Beam Interactions with Materials and Atoms 303 (2013) 104–107.
[19] X.-.M. Bai, A.F. Voter, R.G. Hoagland, M. Nastasi, B.P. Uberuaga, Efficient annealing of radiation damage near grain boundaries via interstitial emission, Science 327 (2010) 1631–1634.
[20] F. Hatami, S.A.H. Feghhi, A. Arjhangmehr, A. Esfandiarpour, Interaction of primary cascades with different atomic grain boundaries in α-Zr: an atomic scale study, Journal of Nuclear Materials 480 (2016) 362–373.
[21] A. Kedharnath, R. Kapoor, A. Sarkar, Atomistic simulation of interaction of collision cascade with different types of grain boundaries in α-Fe, Journal of Nuclear Materials 523 (2019) 444–457.
[22] C. Lu, T. Yang, K. Jin, G. Velisa, P. Xiu, M. Song, Q. Peng, F. Gao, Y. Zhang, H. Bei, Enhanced void swelling in NiCoFeCrPd high-entropy alloy by indentation-induced dislocations, Materials Research Letters 6 (2018) 584–591.
[23] P.P. Cao, H. Wang, J.Y. He, C. Xu, S.H. Jiang, J.L. Du, X.Z. Cao, E.G. Fu, Z.P. Lu, Effects of nanosized precipitates on irradiation behavior of CoCrFeNi high entropy alloys, J Alloys Compd 859 (2021) 158291.
[24] H.-.S. Do, B.-.J. Lee, Origin of radiation resistance in multi-principal element alloys, Sci Rep 8 (2018) 1–9.
[25] Y. Li, R. Li, Q. Peng, Enhanced surface bombardment resistance of the CoNiCrFeMn high entropy alloy under extreme irradiation flux, Nanotechnology 31 (2019) 25703.
[26] Y. Lin, T. Yang, L. Lang, C. Shan, H. Deng, W. Hu, F. Gao, Enhanced radiation tolerance of the Ni-Co-Cr-Fe high-entropy alloy as revealed from primary damage, Acta Mater 196 (2020) 133–143.
[27] Y. Li, R. Li, Q. Peng, S. Ogata, Reduction of dislocation, mean free path, and migration barriers using high entropy alloy: insights from the atomistic study of irradiation damage of CoNiCrFeMn, Nanotechnology 31 (2020) 425701.
[28] Y.-.K. Dou, H. Cao, X.-.F. He, J. Gao, J. Cao, W. Yang, Interaction mechanism of an edge dislocation with a void in Fe–Ni–Cr concentrated solid-solution alloy, J Alloys Compd 857 (2021) 157556.
[29] S. Zhao, Y. Osetsky, Y. Zhang, Atomistic simulation of defect-dislocation interactions in concentrated solid-solution alloys, Physical Review Materials 3 (2019) 103602.
[30] S. Heredia-Avalos, C.D. Denton, J.C. Moreno-Marín, E. Martinez, M.J. Caturla, Collision cascade effects near an edge dislocation dipole in alpha-Fe: induced dislocation mobility and enhanced defect clustering, Journal of Nuclear Materials 543 (2021) 152459.
[31] E.J. Pickering, A.W. Carruthers, P.J. Barron, S.C. Middleburgh, D.E.J. Armstrong, A.S. Gandy, High-Entropy Alloys for Advanced Nuclear Applications, Entropy 23 (2021) 98.
[32] Q. Peng, F. Meng, Y. Yang, C. Lu, H. Deng, L. Wang, S. De, F. Gao, Shockwave generates< 100 >dislocation loops in bcc iron, Nat Commun 9 (2018) 1–6.
[33] A.E. Sand, J. Byggmästar, A. Zitting, K. Nordlund, Defect structures and statistics in overlapping cascade damage in fusion-relevant bcc metals, Journal of Nuclear Materials 511 (2018) 64–74.
[34] E. Zarkadoula, G. Samolyuk, W.J. Weber, Two-temperature model in molecular dynamics simulations of cascades in Ni-based alloys, J Alloys Compd 700 (2017) 106–112.
[35] P. Hirel, Atomsk: a tool for manipulating and converting atomic data files, Comput Phys Commun 197 (2015) 212–219.
[36] Z. Lu, L. Xu, T. Chen, L. Tan, H. Xu, Interactions between displacement cascade and dislocation and their influences on Peierls stress in Fe-20Cr-25Ni alloys, Computational Materials Science 160 (2019) 279–286.
[37] H. Wang, J.-.T. Tian, W. Zhou, X.-.F. Chen, B. Bai, J.-.M. Xue, Collision cascades interact with an edge dislocation in bcc Fe: a molecular dynamics study, RSC Adv 8 (2018) 14017–14024.
[38] S. Plimpton, Fast parallel algorithms for short-range molecular dynamics, J Comput Phys 117 (1995) 1–19.
[39] O.R. Deluigi, R.C. Pasianot, F.J. Valencia, A. Caro, D. Farkas, E.M. Bringa, Simulations of primary damage in a High Entropy Alloy: probing enhanced radiation resistance, Acta Mater 213 (2021) 116951.
[40] D. Farkas, A. Caro, Model interatomic potentials and lattice strain in a high-entropy alloy, J Mater Res 33 (2018) 3218–3225.
[41] X.F. Wang, Y. Zhang, Y. Qiao, G.L. Chen, Novel microstructure and properties of multicomponent CoCrCuFeNiTix alloys, Intermetallics 15 (2007) 357–362.
[42] A. Stukowski, Visualization and analysis of atomistic simulation data with OVITO–the Open Visualization Tool, Modelling and Simulation in Materials Science and Engineering 18 (2009) 15012.